Conformation of a Peptide Corresponding to T4 Lysozyme Residues 59–81 by NMR and CD Spectroscopy†

Michael J. McLeish,*,‡ Katherine J. Nielsen,‡ Lidia V. Najbar,‡ John D. Wade,§ Feng Lin,§ Michael B. Doughty,∥ and David J. Craik*,‡

School of Pharmaceutical Chemistry, Victorian College of Pharmacy, Monash University, 381 Royal Parade, Parkville, Victoria 3052, Australia, Howard Florey Institute, University of Melbourne, Parkville, Victoria 3052, Australia, and Department of Medicinal Chemistry, School of Pharmacy, University of Kansas, Lawrence, Kansas 66045

Received April 28, 1994; Revised Manuscript Received July 1, 1994®

ABSTRACT: The conformation, in solution, of a peptide corresponding to residues 59–81 from T4 lysozyme [LYS(59–81)] has been determined by ^{1}H NMR and CD spectroscopy. This peptide spans the region corresponding to helix C in the crystal structure of T4 lysozyme. Secondary structure predictions indicated that the peptide would possibly be helical in an aqueous environment, but in a more hydrophobic environment the peptide would certainly adopt a helical conformation. This prediction was confirmed by the far-UV CD and NMR studies, which showed the peptide to be relatively unstructured in aqueous solution and significantly helical in the presence of either TFE or SDS micelles, although the ^{1}H NMR results did give some indication of the presence of nascent helix in aqueous solution. For LYS(59–81), in TFE, the three-dimensional structure derived from the NMR data showed that the helix had a more pronounced curvature than the gradual bend observed in the crystal structure.

T4 lysozyme is a small (M_r 18 300), monomeric protein that has a stable and well-characterized structure (Figure 1). The enzyme consists of two domains linked by a long α-helical segment (Weaver & Matthews, 1987), is readily crystallized, and is amenable to site-directed mutagenesis. It contains two cysteine residues but no disulfide bonds. A two-state equilibrium exists between the folded and unfolded forms of the enzyme (Chen *et al.*, 1992). This combination of properties has resulted in T4 lysozyme (and its mutants) being the subject of numerous studies of protein folding (Chen *et al.*, 1992; Ladbury *et al.*, 1992; Lu & Dahlquist, 1992), and stability [for a review, see Matthews (1993)].

The study of Lu and Dahlquist (1992), in particular, provides information about the early events in the folding of T4 lysozyme. In that study, quenched-flow hydrogen–deuterium exchange experiments were combined with two-dimensional NMR spectroscopy to probe for the presence of secondary structure in the partially folded protein. Their results indicated that helix E (corresponding to residues 93–105) was formed earliest during refolding and that helix A (residues 3–8) and a region of β-turn and β-sheet (residues 14–34) rapidly followed. In addition, some amide protons in the long central helix (helix C, residues 60–79) showed protection from exchange. The overall interpretation of these results was that secondary structure certainly was forming prior to any tertiary structure, thereby lending support to the framework (Kim & Baldwin, 1982) and/or molten-globule (Kuwajima, 1989; Ptitsyn, 1987; Ptitsyn *et al.*, 1990) models for protein folding, rather than the subdomain model (Oas & Kim, 1988; Staley & Kim, 1990).

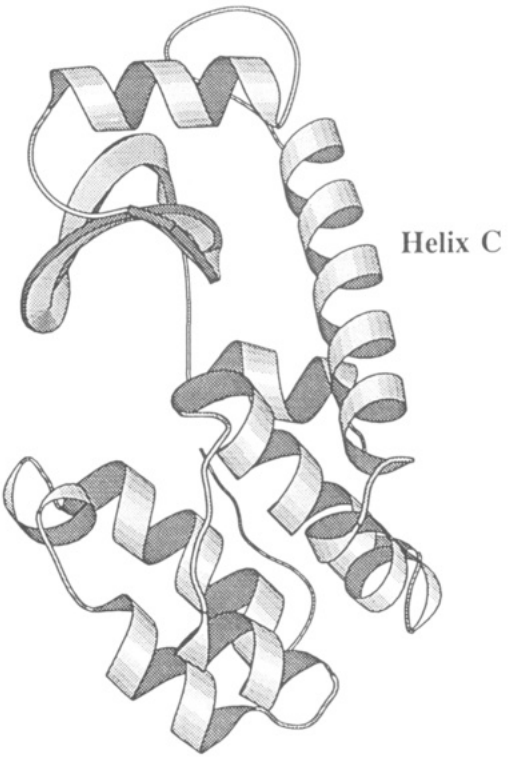

FIGURE 1: Crystal structure of T4 lysozyme generated by Molscript (Kraulis, 1991) showing helix C bridging the two domains.

Similar experiments have been carried out on a variety of proteins, including RNase A (Udgaonkar & Baldwin, 1988), cytochrome *c* (Roder *et al.*, 1988), barnase (Bycroft *et al.*, 1990), and hen egg white lysozyme (Miranker *et al.*, 1991). In each case it was possible to detect the presence of intermediates with some measure of native secondary structure. It is reasonable to propose that these elements of secondary structure should also be stable as isolated peptides. Indeed, this has proved to be the case, as stable α-helices have been observed for several peptides based on native sequences, including the C peptide of ribonuclease A (Brown & Klee,

† The peptide synthesis studies at the Howard Florey Institute were supported by an Institute Block Grant from the National Health and Medical Research Council of Australia. The assistance of the Victorian Education Foundation in providing a postgraduate scholarship (to L.V.N.) is gratefully acknowledged.

* Authors to whom correspondence should be addressed.
‡ Victorian College of Pharmacy.
§ Howard Florey Institute.
∥ University of Kansas.

® Abstract published in *Advance ACS Abstracts,* August 15, 1994.

0006-2960/94/0433-11174$04.50/0

1971; Shoemaker *et al.*, 1987), the Pα5 peptide corresponding to the α-helix of BPTI (Goodman & Kim, 1989), and the C-terminal peptide of cytochrome *c* (Kuroda, 1993). In other cases, secondary structure could be induced by the addition of helix-promoting solvents such as TFE[1] (Segawa *et al.*, 1991; Dyson *et al.*, 1992; Sönnichsen *et al.*, 1992), but generally this only occurs in peptides with a tendency toward helix formation (Segawa *et al.*, 1991; Dyson *et al.*, 1992; Sönnichsen *et al.*, 1992). SDS micelles too have proven useful for stabilizing peptides with helical propensity (Wu & Yang, 1978; Endo *et al.*, 1989; Mammi & Peggion, 1990; Motta *et al.*, 1991), and it has been suggested that strong association between the hydrophobic helical cores of these peptides and the hydrocarbon chains of the SDS micelles is responsible for the enhancement of helix stability (Rizo *et al.*, 1993).

In an earlier study (McLeish *et al.*, 1993), we reported that a peptide corresponding to the 13 N-terminal residues of T4 lysozyme, which includes helix A, was able to form an α-helix in the presence of SDS micelles. This supported the hypothesis that helix A could provide a nucleation site for the folding of the rest of the protein. In the present study, we have used CD and NMR spectroscopy to examine the solution structure of LYS(59–81), a peptide that encompasses the helical segment (helix C, Figure 1) connecting the two domains of T4 lysozyme. In contrast to helix A, whose amide protons showed a high degree of protection from H–D exchange, only a few residues of helix C showed protection from exchange (Lu & Dahlquist, 1992). Nonetheless, given its role in providing support for the positioning of the two domains, and also given that the helix spans more than five turns, it may be expected that LYS(59–81) would have a propensity toward helix formation.

MATERIALS AND METHODS

Peptide Synthesis. The peptide TKDEAEKLFNQDVDAAVRGILRN was assembled on an ABI 430A peptide synthesizer using the protocols described for the synthesis of A-human ANF (Wade *et al.*, 1986). Side-chain protection was as follows: Arg (Tos), Asp (OcHex), Glu (OBzl), Lys (Cl-Z), and Thr (Bzl). The peptide was cleaved from the resin and simultaneously deprotected using 90% HF/10% *p*-cresol for 1 h at 0 °C. The crude peptide was extracted into 10% aqueous acetic acid, diluted with water, lyophilized, and then purified by reversed-phase HPLC using aqueous TFA-containing acetonitrile gradients. The overall yield of purified peptide was 27%. Amino acid analysis of a 24 h acid hydrolyzate gave the following results, with the theoretical values in parentheses: Asx (5), 5.15; Thr (1), 0.96; Glx (3), 3.28; Gly (1), 1.09; Ala (3), 2.94; Val (2), 2.04; Ile (1), 0.98; Leu (2), 1.94; Phe (1), 0.96; Lys (2), 1.85; and Arg (2), 1.86. Additional characterization by reversed-phase HPLC and by capillary zone electrophoresis at pH 2.5 provided further confirmation of the high purity of the peptide.

Secondary Structure Predictions. The conformational preferences of LYS(59–81) were simulated using the program ALB (Ptitsyn & Finkelstein, 1983). This program predicts elements of secondary structure on the basis of the physical properties of polypeptides when they are placed in aqueous, partially hydrophobic, and fully hydrophobic environments.

CD Spectropolarimetry. CD spectra were recorded on an AVIV 60DS spectropolarimeter. The instrument was calibrated using *d*-10-camphorsulfonic acid. Cells having a path length of either 0.1 or 0.02 cm were employed and were maintained at the required temperature using a Lauda circulating water bath. Peptide concentrations were between 50 and 800 μM and were determined by amino acid analysis. Spectra were averages of five scans recorded with a bandwidth of 1 nm, a 0.25 nm step size, and a 0.2 s time constant. Following baseline correction, the observed ellipticity was converted to a mean residue ellipticity, $[\theta]$ (deg·cm^2 dmol^{-1}), using the relationship $[\theta] = \theta/(lcN)$, where θ is the observed ellipticity, l is the path length in millimeters, c is the molar concentration, and N is the number of residues in the peptide. The spectra were then smoothed using a third-order polynomial function.

^{1}H NMR Spectroscopy. Peptides were prepared to a final concentration of 2 mM in a volume of 0.6 mL. The aqueous component for all samples was maintained at the desired pH with 0.1 M phosphate buffer. Samples were prepared in 90% H_2O/10% D_2O (pH 5.0, 281 K), 50% TFE/50% buffer (pH 5.0, 278 K), or 200 mM deuterated SDS micelles/90% H_2O/10% D_2O (pH 4.0, 303 K). For the slow exchange experiments, samples were prepared in 100% D_2O, 50% TFE-d_3/50% D_2O, or 200 mM SDS-d_{25}/100% D_2O.

The 2D experiments included DQF-COSY (Rance *et al.*, 1983), TOCSY (Braünschweiler & Ernst, 1983; Davis & Bax, 1985) using a DIPSI spin–lock sequence (Cavanagh & Rance, 1992) with a mixing time of 65 ms, and NOESY (Kumar *et al.*, 1980) with mixing times ranging from 100 to 500 ms. For DQF-COSY spectra, the water resonance was suppressed by gated irradiation during the relaxation delay (1.5–2 s), while the transmitter offset was placed to coincide with the water resonance. Solvent suppression for NOESY and TOCSY experiments was achieved using a 1–1 binomial pulse sequence in place of the final 90° pulse (Plateau & Gueron, 1982), in combination with mild presaturation. Spectra were routinely acquired with 4K complex data points in F_2 and 400–600 increments in the F_1 dimension, of 32 scans each (80 for NOESY).

All data were processed using UXNMR (Bruker) and FELIX (Hare Research Inc.) software. The t_1 dimension was zero-filled to 2048 real data points, and 60° phase-shifted sine bell window functions were applied. Polynomial baseline correction was applied in selected regions of the spectra. Chemical shifts were referenced to internal 2,2-dimethyl-2-silapentane-5-sulfonate (DSS) at 0.0 ppm.

Peak volumes in the 100 ms 50% TFE/50% H_2O NOESY spectra were classified as strong, medium, or weak corresponding to upper bound interproton distance restraints of 2.7, 3.5, and 5.0 Å, respectively (Clore *et al.*, 1986). Pseudoatom corrections were applied to non-stereospecifically assigned methylene or methyl protons (Wüthrich *et al.*, 1983), and 1.5 Å was added to the upper limits of distances involving methyl protons.

Structure Calculations. 3D structures were generated using XPLOR (version 3.0; Brünger *et al.*, 1986; Brünger, 1992). An *ab initio* simulated annealing protocol was used (Nilges *et al.*, 1988), starting from a template structure with randomized coordinates, to generate a set of 40 structures. The simulated annealing protocol consisted of 20 ps of high-

[1] Abbreviations: LYS(59–81), peptide corresponding to TH lysozyme residues 59–81; CD, circular dichroism; NMR, nuclear magnetic resonance; TFE, 2,2,2-trifluoroethanol; SDS, sodium dodecyl sulfate; NOE, nuclear Overhauser effect; NOESY, two-dimensional nuclear Overhauser spectroscopy; TOCSY, total correlation spectroscopy; COSY, two-dimensional correlated spectroscopy; DQF-COSY, double-quantum-filtered COSY; DIPSI, decoupling in the presence of scalar interactions; DSS, 4,4-dimethyl-4-silapentane-1-sulfonate; FID, free induction decay; 2D, two-dimensional; 3D, three-dimensional; RMSD, root mean square deviation.

Table 1: Secondary Structure Prediction for LYS(59–81)[a,b]

	T	K	D	E	A	E	K	L	F	N	Q	D	V	D	A	A	V	R	G	I	L	R	N
Aqueous			N	P	P	P	P	P	P	N	N	N	H	H	H	H	H	H	H	H	N	N	
Partially Hydrophobic			N	P	P	H	H	H	H	N	N	N	H	H	H	H	H	H	H	H	N	N	
Fully hydrophobic				P	H	H	H	H	H	N	N	N	H	H	H	H	H	H	H	H	H	N	

[a] Calculated using the ALB algorithm (Ptitsyn & Finkelstein, 1983), with T = 288 K and pH 5.0. [b] H, helix predicted; P, probable helix; N, helix not predicted.

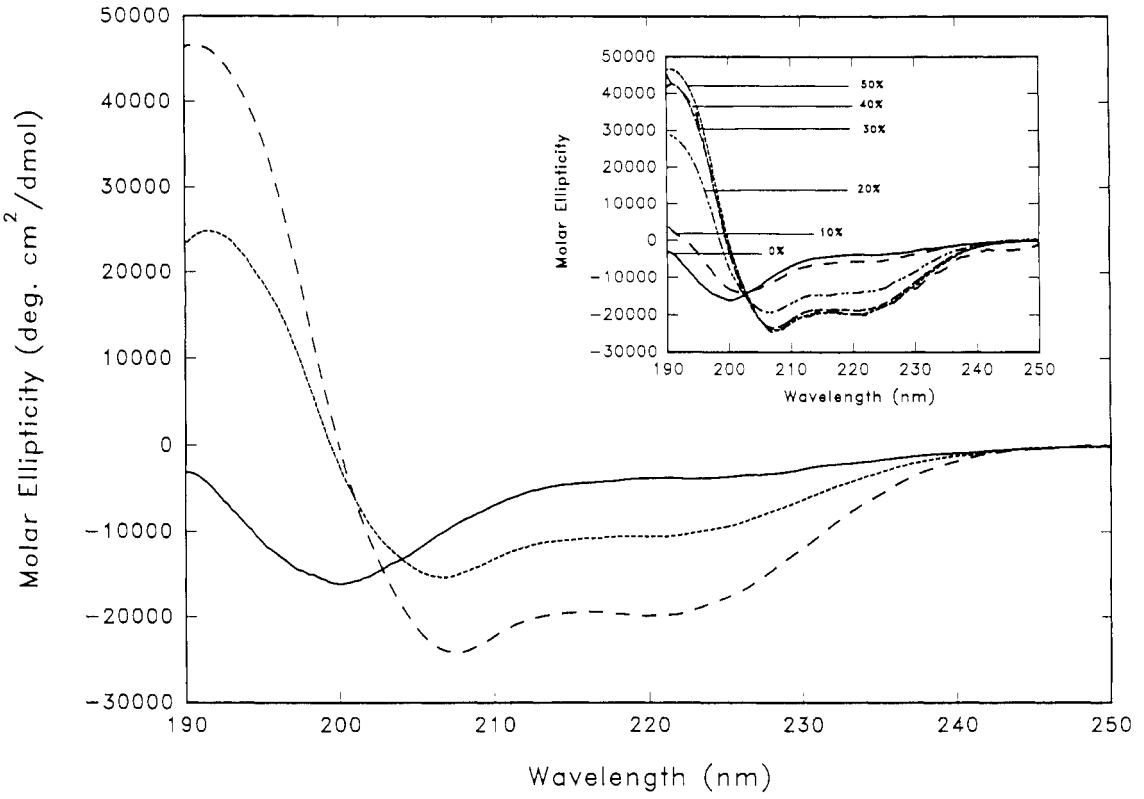

FIGURE 2: CD spectra of LYS(59–81) at 288 K in (—) 10 mM phosphate buffer (pH 4.8), (···) SDS micelles (200 mM), and (– –) 50% TFE. The inset shows increasing helicity as the TFE concentration is increased.

temperature molecular dynamics where the initial atom velocities were chosen from a Maxwellian distribution at 800 K. Initially, this was performed with a low weighting on all NOE restraints and a low weighting on the repel force constant, which allows all atoms to pass through each other. This was followed for an additional 10 ps with an increased force constant on experimental NOE restraints. The dihedral force constant was increased prior to cooling the system to 300 K and increasing the repel force constant over 15 ps in 5 fs steps. Structure refinement was achieved using the conjugate gradient Powell algorithm with 400 cycles of energy minimization (Clore et al., 1986) and a refined force field based on the program CHARMM (Brooks et al., 1983). Final structures were superimposed and viewed using INSIGHT (Biosym), and geometric analyses on the refined structures were performed within XPLOR.

RESULTS

Structure Prediction. Table 1 shows the secondary structure predicted by the program ALB (Ptitsyn & Finkelstein, 1983) for LYS(59–81) in an aqueous environment, a partially hydrophobic environment, and a fully hydrophobic environment. Simulations were carried out at 288 K at a pH of 5.0. Overall, a high degree of helicity was predicted, even in an aqueous environment where a helix was predicted between residues 13 and 21, with residues 4–9 also showing a propensity toward helix formation. As the hydrophobicity was increased, the predicted helix region was found to extend from residue 5 to 21, with the exception of residues 10–12 where no helix was predicted under any conditions.

CD Spectropolarimetry. Figure 2 shows the CD spectra of LYS(59–81) at 288 K in 10 mM phosphate buffer (pH 4.8), in SDS micelles (250 mM), and in varying concentrations

Table 2: CD Determination of α-Helix Content for LYS(59–81)[a]

solvent	$[\theta]_{222}$[b]	PROSEC	LINCOMB[d]
10 mM KPO_4 (pH 4.8)	10.8	0.0	0.0
10% TFE	16.6	2.1	12.7
20% TFE	39.4	25.0	30.1
30% TFE	53.0	40.2	43.1
40% TFE	57.1	42.1	45.3
50% TFE	55.8	44.7	46.6
200 mM SDS	32.0	25.4	39.7

[a] CD data were collected at 15 °C, at peptide concentrations between 50 and 800 μM. [b] Calculated using the method of Chen *et al.* (1974). [c] Calculated by fitting data, using the program PROSEC, to the reference spectra of Yang *et al.* (1986). [d] Calculated by fitting data using the program of LINCOMB, which employs a convex constraint method of analysis (Perczel *et al.*, 1992).

of TFE. The spectrum in aqueous solution is consistent with the peptide being primarily unstructured, although the minimum just above 200 nm and a degree of negative ellipticity at 222 nm give an indication that some structure may be present (Woody, 1985). The addition of the structure-inducing solvent, TFE, induces a shift toward helical conformation. By 50% TFE, the minimum has shifted to 208 nm ($\pi\pi^*$ transition) and considerable negative ellipticity has developed at 222 nm ($n\pi^*$ transition). The inset to Figure 2 shows an isodichroic point (at ca. 203 nm) indicative of a transition between two conformational states; random coil and α-helix (Padmanabhan *et al.*, 1990; Zhou *et al.*, 1993). The shift toward a helical structure in a hydrophobic environment is also evident in SDS, with minima arising at 207 and 222 nm, but the extent of helix formation clearly is lower. The CD spectra, obtained at peptide concentrations between 50 and 800 μM, were essentially identical, suggesting that aggregation was not occurring.

If we assume that the absorption at 222 nm is due to α-helix almost exclusively (Woody, 1985), it is possible to calculate the degree of α-helicity using the equation of Chen *et al.* (1974):

$$[\theta]_\lambda = (f_H - ik/N)[\theta]_{H\lambda_\infty}$$

where $[\theta]_\lambda$ is the observed mean residue ellipticity at wavelength λ, f_H is the fraction of helix, i is the number of helical segments (1 in this case), k is a wavelength-dependent constant, N is the number of residues, and $[\theta]_{H\lambda_\infty}$ is the maximum mean residue ellipticity for a helix of infinite length. On this basis, the $[\theta]_{222}$ for LYS(59–81) in a 100% helical conformation was calculated to be −35 100 deg·cm^2 dmol^{-1}. The helicity of the peptide in each solvent, expressed as a percentage, determined on the basis of the mean residue ellipticity at 222 nm is shown in Table 2. Helicity values of 11%, 32%, and 56% for aqueous solution, SDS micelles, and 50% TFE, respectively, clearly demonstrate the ability of the latter two solvents to stabilize secondary structure.

There are potential difficulties in estimating helicity from $[\theta]_{222}$ data due to inaccuracies in determining peptide concentrations and small shifts in wavelength (Bruch *et al.*, 1991). For comparison with the results obtained from $[\theta]_{222}$ data, we used two other approaches to estimate secondary structure from the CD data. The first utilized the curve-fitting program PROSEC (Aviv Co.), which is based on the algorithm and basis spectra of Yang *et al.* (1986). The second employed the program LINCOMB (Perczel *et al.*, 1992) and used a reference curve set containing five pure-component curves (Perczel *et al.*, 1992). In the latter method, the reference curves were derived using convex constraint analysis of 25 CD spectra obtained from 25 different proteins (Perczel *et al.*, 1992). Helicity data from the LINCOMB method were calculated after the contribution attributed to aromatic residues was removed. Results from both methods, also shown in Table 2, are in broad agreement with those obtained from the $[\theta]_{222}$ data but, in general, provide a somewhat lower estimate of helicity.

The effect of temperature on the conformation of LYS-(59–81) in 50% TFE and in SDS micelles is shown in Figure 3A,B, respectively. As the temperature increases, a concomitant decrease in ellipticity at 222 nm is observed, consistent with a loss of helicity. In both cases a clear isodichroic point is seen, again indicating the presence of a helix/random coil transition. Similar spectra have been observed for other small peptides that partially populate helical conformations (Padmanabhan *et al.*, 1990; Zhou *et al.*, 1993; Waltho *et al.*, 1993).

NMR Spectroscopy. Peptide samples were prepared to produce optimal conditions for helix formation. For example, low temperatures (278–281 K) were used, when possible, to reduce the amount of conformational averaging in solution. As SDS is insoluble over this temperature range, samples containing SDS were maintained at 303 K. The pH values of the samples were also adjusted to maximize helix stability. For LYS(59–81) in TFE and aqueous solutions, the pH was maintained at 5 so that side-chain COOH groups (i.e., aspartate and glutamate) were predominantly charged. It was anticipated that this would enhance any salt bridge formation between positively and negatively charged side chains for residues i and $i + 4$ along the sequence (i.e., K2–E6, D3–R7, D14–R18). In SDS, negatively charged side

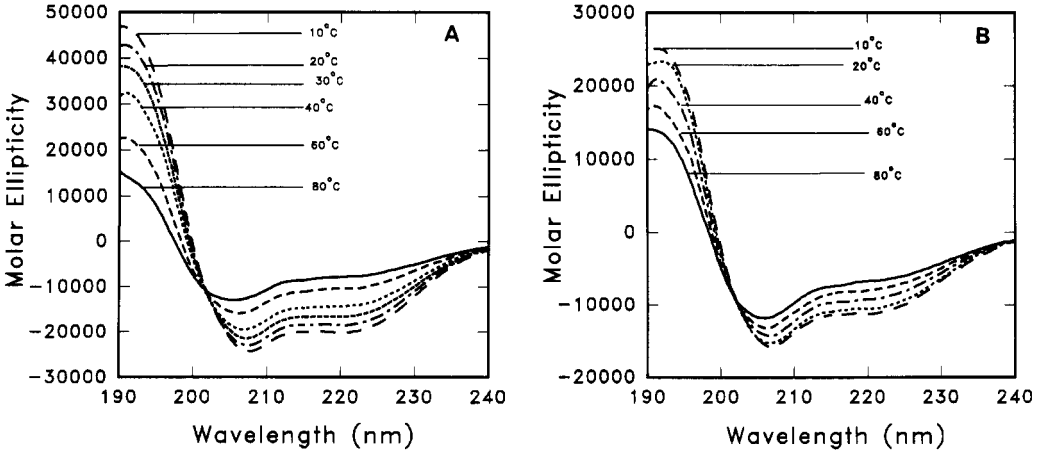

FIGURE 3: Effect of temperature on the conformation of LYS(59–81) in (A) 50% TFE and (B) SDS micelles.

Table 3: ^{1}H NMR Chemical Shifts (ppm) and Resonance Assignments for LYS(59–81) in H_2O at 281 K and pH 5.0 (HDO = 4.96 ppm)

residue	NH	Hα	Hβ	others
Thr1		4.19	3.89	γCH_3, 1.48
Lys2	8.94	4.29	1.76, 1.79	γCH_2, 1.39; δCH_2, 1.63; ϵCH_2, nd[a]
Asp3	8.55	4.52	2.58, 2.68	
Glu4	8.35	4.17	1.91, 2.01	γCH_2, 2.25
Ala5	8.37	4.19	1.38	
Glu6	8.32	4.12	1.96, 2.21	γCH_2, 2.30
Lys7	8.23	4.19	1.72	γCH_2, 1.32; δCH_2, nd; ϵCH_2, 2.92
Leu8	8.14	4.25	1.55	γCH_2, 1.40; δCH_3, 0.77, 0.84
Phe9	8.24	4.54	3.01, 3.08	2,6-H, 7.20; 3,4,5-H, 7.29
Asn10	8.42	4.57	2.58, 2.7	
Gln11	8.37	4.20	1.95, 2.08	γCH_2, 2.30
Asp12	8.41	4.56	2.66, 2.75	
Val13	8.08	3.97	2.04	γCH_3, 0.89
Asp14	8.37	4.53	2.58, 2.70	
Ala15	8.17	4.11	1.38	
Ala16	8.24	4.20	1.37	
Val17	7.95	4.00	2.09	γCH_3, 0.88, 0.93
Arg18	8.24	4.25	1.83	γCH_2, 1.76; δCH_2, nd; δNH, 7.25
Gly19	8.33	3.90		
Ile20	7.96	4.10	1.80	γCH_2, 1.11, 1.36; γCH_3, 0.84; δCH_3, 0.82
Leu21	8.37	4.34	1.61	γCH_2, 1.52; δCH_3, 0.82, 0.88
Arg22	8.44	4.34	1.71, 1.85	γCH_2, 1.59; δCH_2, 3.15; δNH, 7.23
Asn23		4.42	8.11	

[a] nd, not determined.

chains are not desirable due to electrostatic repulsion from the negatively charged micelle exterior (see following); consequently, a lower pH was used.

(A) Chemical Shift Assignments. The ^{1}H NMR spectra for LYS(59–81) in H_2O and in 50% TFE solutions show good peak dispersion. The resonance assignments therefore were relatively straightforward, using well-established techniques (Wüthrich, 1986). TOCSY and DQFCOSY spectra were used to identify the individual spin systems, and NOESY spectra were used to complete the sequential assignments. The ^{1}H NMR spectra for the SDS samples were more overlapped, making resonance assignment difficult. Furthermore, the TOCSY spectra for these solutions had poor signal-to-noise, a characteristic that has been previously noted for peptide/micelle systems (McLeish *et al.*, 1993; Rizo *et al.*, 1993) and may be attributed to the large effective correlation time experienced by the peptide upon association with the micelle. The assignment of LYS(59–81) in SDS solution was achieved primarily by the analysis of NOESY spectra recorded under varied conditions of pH and temperature. When the SDS samples were buffered at pH 5, the NOESY spectra were poor, few NH–NH_{i+1} connectivities were observed, and most peaks were not assignable. At pH 4, the quality of the NOESY spectrum was greatly improved, several NH–NH_{i+1} connectivities were observed, and full peak assignment was possible. Presumably, the lower degree of negative charge on the peptide resulted in a more favorable interaction with the micelles at the lower pH.

Table 3 shows the complete resonance assignments of LYS(59–81) in H_2O. NOESY spectra that illustrate sequential assignment in H_2O and TFE are shown in Figure 4. The NOE cross peaks for the TFE (Figure 4B) and SDS spectra (data not shown) are much stronger than those for the aqueous spectra, and fewer peaks are observed in H_2O (Figure 4A) even at very long mixing times (500 ms). This indicates that LYS(59–81) has a shorter correlation time (τ_c) in H_2O than in SDS or TFE. In SDS, the larger number of NOEs observed at shorter mixing times (≤200 ms) indicates that the connectivities primarily are due to SDS-bound peptide. In TFE, many NOEs are observed at very low mixing times (100 ms), suggesting that LYS(59–81) is highly structured in this cosolvent.

(B) Secondary Structure. The deviations from aqueous random coil values (Wishart et al., 1991) for the Hα, NH, and Hβ chemical shifts of LYS(59–81) in H_2O, SDS, and TFE are presented in Figure 5. For LYS(59–81) in aqueous solution, the series of shifts upfield from random coil values is consistent with the presence of some α-helix from residues 3–19. The chemical shifts of LYS(59–81) are substantially affected by solution environment. The upfield Hα chemical shift changes indicate an increase in helicity for LYS(59–81) in TFE and SDS by comparison with the H_2O data. This is consistent with findings that these solvent conditions are conducive to helix stabilization in peptides with inherent propensities for helix formation (Wu et al., 1982; Sönnichsen et al., 1992). The NH chemical shifts, which are generally sensitive to solvent conditions, pH, and temperature, are subject to a mild periodic fluctuation. Amide chemical shift periodicity has previously been identified in other amphipathic helical peptides (Kuntz et al., 1991; Jiménez et al., 1992;

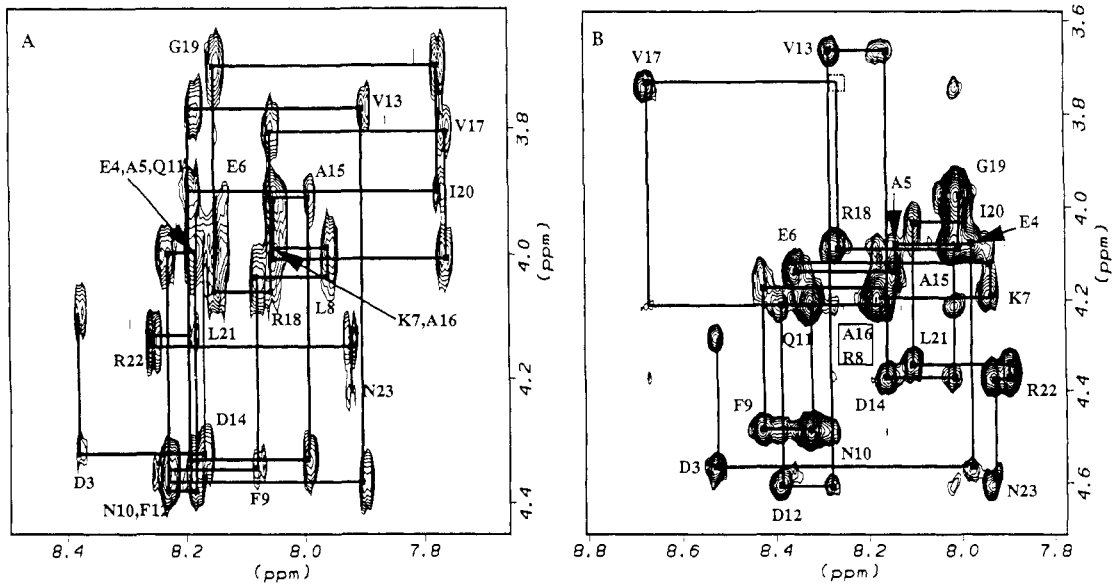

FIGURE 4: NH–αH regions of NOESY spectra for LYS(59–81) in (A) 90% H_2O/10% D_2O at pH 5.0 and 281 K and (B) 50% TFE/50% buffer at pH 5.0 and 278 K. Mixing times are 300 and 100 ms, respectively.

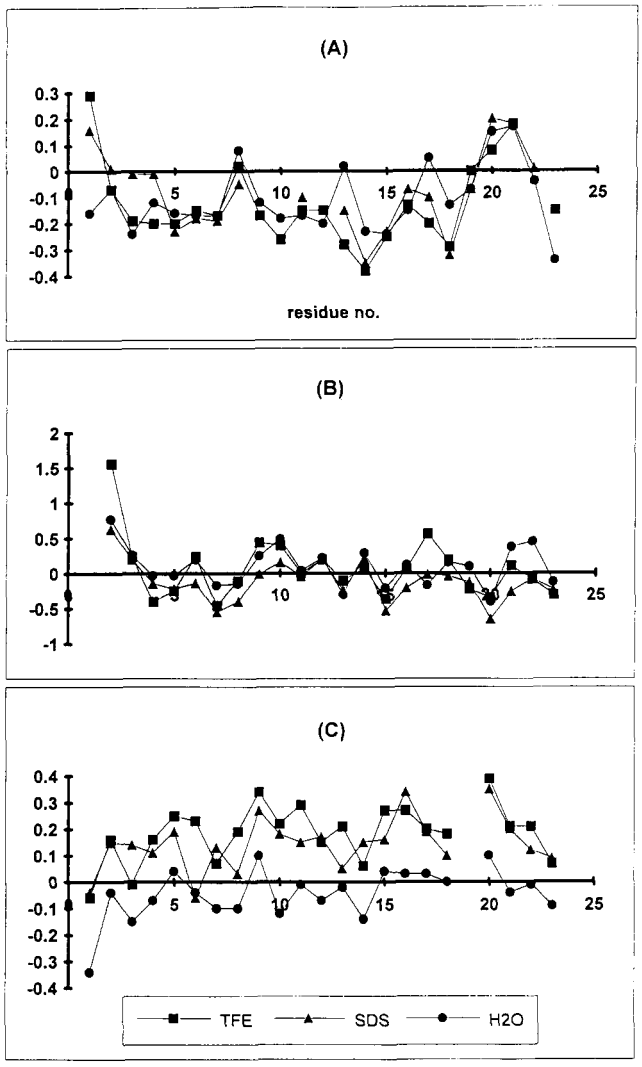

FIGURE 5: Deviations from aqueous random coil values (vertical axis) versus residue number (horizontal axis) for the (A) Hα, (B) NH, and (C) Hβ chemical shifts of LYS(59–81) in H_2O, SDS micelles, and TFE.

Zhou et al., 1992) and is taken to indicate a curved helical structure. The most pronounced chemical shift changes are observed for the Hβ protons, which are close to random coil values in aqueous solution, but are shifted downfield considerably in SDS and, to a greater extent, in TFE, indicating that the helicity of LYS(59–81) is increased in these solvents.

Summaries of the sequential and medium-range NOEs for LYS(59–81) in H_2O, SDS, and TFE solutions are depicted in Figure 6A–C, respectively. In H_2O, the NH–NH_{i+1} connectivities are weaker than the corresponding Hα–NH_{i+1} connectivities, suggesting that for LYS(59–81) any helix present is in equilibrium with partially unfolded and/or extended conformations in aqueous solution. However, the presence of one Hα–NH_{i+2} connectivity and several Hα–$H\beta_{i+3}$ connectivities of medium strength along the region encompassed by residues 4–20 indicates that at least nascent helical structures are present in this medium (Dyson & Wright, 1991). This region corresponds with the helical region suggested by the Hα chemical shift analysis. In support of this, several slow (present ≥4 h) and moderately slow exchange (present 0.5–2 h) NH protons are observed along the stretch 3–22, indicating the presence of H-bonds. Furthermore, several $^3J_{NH-H\alpha}$ coupling constants were measured at ≤6 Hz (residues 6–9 and 13–21), indicating that extended populations are not present in significant amounts along these two regions. The

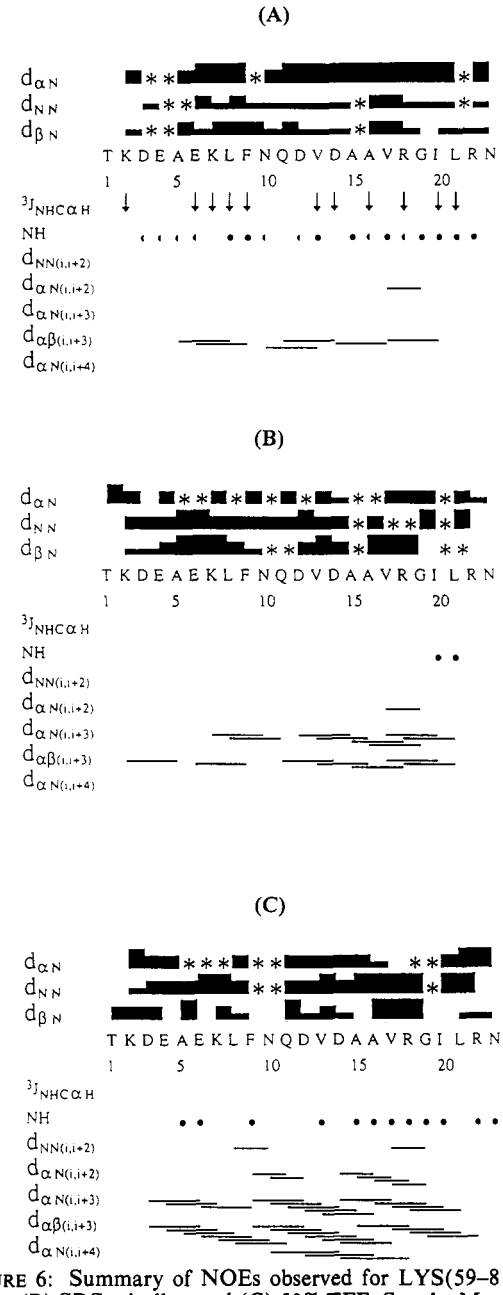

FIGURE 6: Summary of NOEs observed for LYS(59–81) in (A) water, (B) SDS micelles, and (C) 50% TFE. See the Materials and Methods section for solution conditions. Approximate NOE intensities are indicated by the heights of the bars. Overlapping NOEs are indicated by an asterisk (*). Whole and half circles indicate residues for which slow exchange and moderately slow exchange NH protons were observed, respectively. Down arrows indicate $^3J_{NH-H\alpha} \leq 6$ Hz.

regions with low $^3J_{NH-H\alpha}$ coupling constants correspond very well with the regions predicted to form helices in aqueous solution. Interestingly, residues 10–12, which are not predicted to form a helix, had $^3J_{NH-H\alpha}$ coupling constants in the conformational averaging regime of 6–8 Hz.

Nascent helical structures generally are stabilized by the addition of structure-promoting solvents such as TFE (Dyson *et al.*, 1992), and for LYS(59–81), this is certainly the case. The observation of several strong Hα–$H\beta_{i+3}$ and NH–NH_{i+1} connectivities together with weaker Hα–NH_{i+3} and Hα–NH_{i+4} connectivities, suggests that a regular α-helix incorporating residues 2–22 is present (Figure 6B). The presence of a few Hα–NH_{i+2} NOEs is indicative of some populations of 3_{10}-helix. This suggests some degree of partial unfolding as 3_{10}-helices have been identified on the unfolding pathways of

helical peptides (Sundaralingham & Sekharudu, 1989; Tirado-Rives & Jorgensen, 1991).

The presence of helical structures is supported by the observation of 15 slowly exchanging NH protons, of which 12 could be unambiguously identified (Figure 6C). Usually, additional evidence for helix formation can be found by the measurement of low (≤6 Hz) $^3J_{NH-H\alpha}$ coupling constants. However, this information could not be obtained for LYS-(59-81) in TFE, even when peak deconvolution methods were used. This can be attributed to a combination of large peak widths and low coupling constants, as evidenced by the fact that the intensities of the NH–Hα DQF-COSY cross peaks were very low (<20%) in the putative helical regions compared with the NH–Hα peaks for residues near the termini.

Although peak overlap prevented the observation of some connectivities, the summary of observed NOEs for LYS(59–81) in SDS at pH 4 (Figure 6B) shows that, in this environment, some well-defined helix is present from residues 2–22. Supportive evidence for this is provided by the observation of several slowly exchanging NH protons, of which only two were unambiguously identifiable. Again, $^3J_{NH-H\alpha}$ coupling constants were not obtainable because of peak broadening.

Semiquantitative analysis of the NH–NH$_{i+1}$ and Hα–NH$_{i+1}$ NOE intensities via the method of Bradley *et al.* (1990) provides an indication of the amounts of folded versus unfolded species. The results show that there is a significant percentage of folded populations. In H_2O, the global folded content is 65%, and in TFE and SDS, this increases to >90%. In SDS, this information is biased toward the SDS-bound peptide and does not reflect the true global population.

The ^{1}H NMR studies have provided conclusive evidence that, in aqueous solution, LYS(59–81) adopts at least transient helix formations, particularly at residues 6–9 and 13–20. That helix structures exist in the absence of the external hydrophobic effects reflects the strong inherent propensity toward helix formation of the primary sequence in this region of T4 lysozyme. In the hydrophobic environments provided by the TFE and SDS cosolvents, the ^{1}H NMR and CD studies indicate that the helix structure in LYS(59–81) is stabilized. The helix formed in these environments stretches from approximately residues 3–22, with the N- and C-cap regions showing less definition than the core region.

The length of helix determined in TFE solution approximates that defined by the X-ray structure (~5 turns; Weaver & Matthews, 1987), and it is of interest to compare the solution structure of LYS(59–81) to the corresponding region found by X-ray determination.

(C) Three-Dimensional Stucture Calculations. A total of 303 distance constraints derived from 195 intraresidual, 61 sequential, and 47 medium-range NOEs was used in the calculation of 40 simulated annealing (SA) structures. No H-bond or dihedral constraints were used in the SA calculations. All SA runs converged to produce structures with a similar fold. These structures satisfied the experimental constraints, with an average of only three interproton distance violations greater than 0.1 Å per structure. The 20 structures with the lowest energies were used to represent the solution structure of LYS(59–81).

A superimposition of the backbone atoms of residues 3–21 for the 20 refined structures (Figure 7) shows that the helix present from residues 2–22 is well-defined over most residues, apart from some dynamic fraying at the helix termini. The backbone pairwise RMSD for all residues is 2.72 Å, and the average RMSD to the mean structure is 1.82 Å. The quality of the final structures is apparent from Figure 8, which displays

FIGURE 7: Superimposition of the backbone atoms of residues 3–21 for the 20 refined structures derived from experimental NOE data in 50% TFE.

the RMSDs to the averaged structure for each residue and the precision of local backbone and side-chain geometries for each residue using the angular order parameter, S, as a measure of the spread of Φ, Ψ, χ_1, and χ_2 dihedral angles within the structures (Hyberts *et al.*, 1992; Pallaghy *et al.*, 1993). The low RMSDs to the averaged structure show that the backbone structure of LYS(59–81) is best defined from residue 3 to 21. The Φ,Ψ dihedral combinations for the structures show that residues 2–22 consistently lie in the α-region of the Ramachandran plot. The high values of S (mostly ≥0.99), which correspond to a standard deviation of ≤8° for the Φ and Ψ angles of residues 4–21, provide an indication of the precision of the helical structure. Several of the S values for the χ_1 and χ_2 dihedral angles also approach unity (Figure 8D,E), indicating good definition of the side-chains in these regions. The low degree of angular spread between structures means that they are accurately represented by an averaged structure in the helical region.

Analysis of possible H-bond partners for the observed slow exchange NH protons was conducted using SSTRUC [Smith (1991), unpublished program] which identifies H-bonds on the basis of NH···C=O distance and relative orientation using the algorithm of Kabsch and Sander (1983). The results show that, with one exception (at Lys7), the C=O oxygens of residues 2–18 favor the $i,i+4$ H-bond observed in regular α-helices over $i,i+3$ H-bonds. This indicates that regular helix rather than 3_{10}-helix is the dominant folded form in the structural equilibrium.

Some disruption of the helix around Asp12 was suggested by the qualitative NOE analysis, and this is confirmed by the 3D structure calculations. The RMSD values increase at residues 11 and 12 and, correspondingly, the S values for the Φ, Ψ, and χ_1 dihedrals decrease at Gln11 (Figure 8B–D) by comparison with the values for the adjacent regions. These

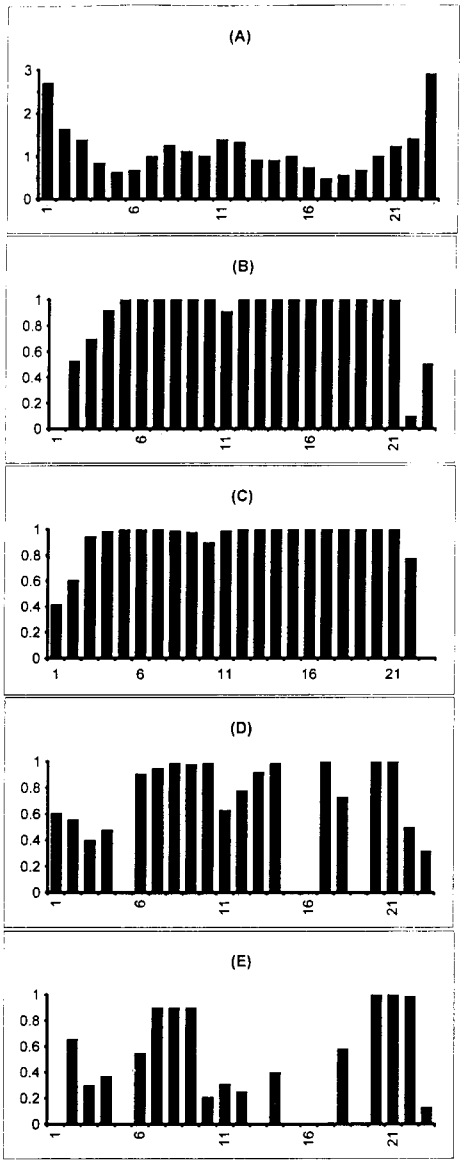

FIGURE 8: (A) RMSD to the average structure (vertical axis) and (B–E) angular order parameter (S) for the Φ, Ψ, χ_1, and χ_2 dihedral angles (vertical axes) for each residue (horizontal axes).

differences are minor and suggest only minimal disruption of the helix in this region.

DISCUSSION

Although the CD results show that LYS(59–81), in water, is largely unstructured, the ^{1}H NMR results indicate that the peptide forms at least transient helical conformations from residues 3–21. Two better defined regions are present at residues 6–9 and, as foreshadowed by the secondary structure predictions (Table 1), 13–21. That the CD measurements did not suggest extensive helical populations was not unexpected, as CD ellipticity values generally are lowered by helix fraying and nonideal helix geometry (Dyson & Wright, 1991). The NMR data indicated that, in water, the global folded content of LYS(59–81) was greater than 60%. The term folded is preferred over helical when estimating structural populations via the NOE-based method of Bradley *et al.* (1990) because, in the conformational ensemble of structures present in the equilibrium, each of the turn, helix and 3_{10}-helical conformations may elicit observable NH–NH$_{i+1}$ NOEs. Other $_1$H NMR methods have been developed to determine either relative or absolute helical populations, including the analysis of $^3J_{NH-H\alpha}$ coupling constants (Bradley *et al.*, 1990) and comparisons of relative Hα–Hβ_{i+3}/Hα_i–Hβ_i and Hα–Hβ_{i+3}/Hα_{i+3}–Hβ_{i+3} NOE strengths (Waltho *et al.*, 1993). However, the results obtained via the NOE method of Bradley *et al.* (1990) provide sufficient evidence to conclude that LYS(59–81) is substantially folded under aqueous conditions.

The CD and NMR data are in accord, in that both show that the degree of helicity of the peptide increases in the more hydrophobic environments provided by SDS and TFE. This observation is consistent with several studies where peptides with inherent helical propensity have been shown to be stabilized by either SDS (Mammi & Peggion, 1990; Rizo *et al.*, 1993) or TFE (Dyson *et al.*, 1992; Sönnichsen *et al.*, 1992; Jasanoff & Fersht, 1994). Although the region containing residues 10–12 is not predicted to form a helix (Table 1), the NMR studies indicate that this region is incorporated into the helical structure, but that it also provides a site for helix disruption.

A comparison of the 3D structures of LYS(59–81) in 50% TFE and the corresponding region in the X-ray structure of T4 lysozyme (Weaver & Matthews, 1987) shows that the extent of helix in these structures is similar. Furthermore, the helical region, which has been shown to consist mostly of regular helix in LYS(59–81), is exclusively regular in the X-ray structure. However, the helix observed in each LYS-(59–81) structure is not linear, but appears curved or kinked. This kink, measured over the well-defined 3–21 region, follows the same direction in all of the calculated structures and is defined by a radius of curvature (R) of approximately 26 Å or a kink at Gln11 of 18°. By comparison, the corresponding region in the T4 lysozyme X-ray structure is more linear, with a bend angle of 8.5° (Sauer *et al.*, 1992). The difference in the curvature of the two helices is demonstrated clearly by the superimposition shown in Figure 9.

Using the definition of Barlow and Thornton (1988), a helix is considered curved when $R \leq 90$ Å or kinked when there is a definite kink site and $R \leq 45$ Å. Curvature in helices can also result from a combination of a kink and a gradual bend over the entire length of the helix, and it is in the latter category that the helix of LYS(59–81) appears to belong. That the curvature is real, and not simply an artifact of 3D structure generation, is supported by several factors. Firstly, the empirical NH chemical shift measurements show a periodicity consistent with a curved helical structure (Zhou *et al.*, 1992). In addition, there were no long-range NOEs of the type observed by Osterhout *et al.* (1989) that could falsely distort a helical structure. The concave face of curvature lies on the more hydrophobic side of the helix, as has been observed for all of the curved helices described by Barlow and Thornton (1988). As a corollary, the NH backbone protons along the hydrophobic face of the helix core are more slowly exchanging in D_2O, presumably because they are less exposed than the corresponding protons along the more hydrophilic face.

It is intriguing that the curvature found in the isolated fragment is more pronounced than in the crystal structure of the native protein. Arguably, either solvent effects are responsible for the kink found in the solution structure of the peptide, or tertiary interactions are responsible for the more linear form of the helix found in the crystal. Support for the former proposal is provided by an analysis of the amide chemical shifts of the native protein in solution (McIntosh *et al.*, 1990), which shows a periodicity not dissimilar to that of the isolated peptide.

A helical wheel representation of LYS(59–81) from residues 2–22 (Figure 10) illustrates the amphipathic nature of the

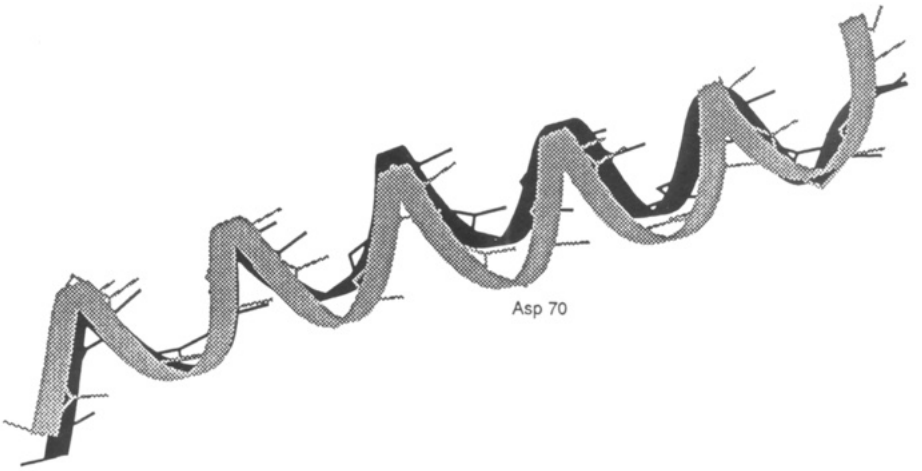

FIGURE 9: Averaged LYS(59–81) structure (black) superimposed on the corresponding region of the crystal structure of T4 lysozyme (gray) highlights the kink observed for the peptide.

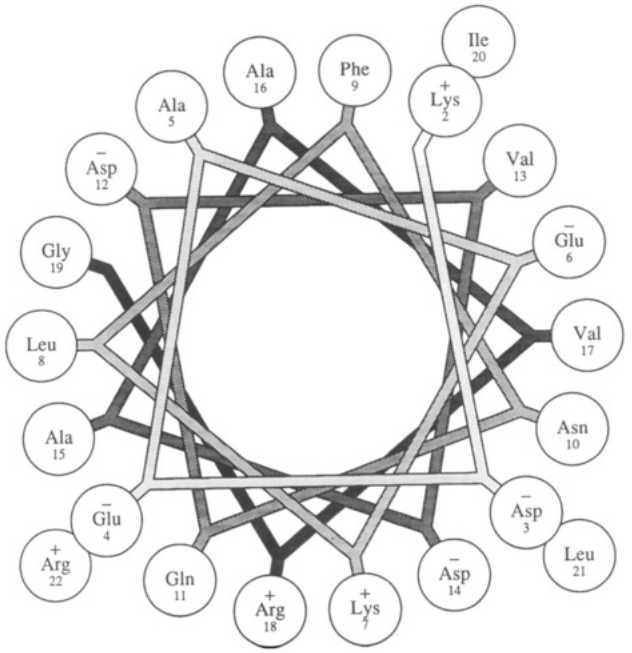

FIGURE 10: Schiffer–Edmundson helical wheel representation of LYS(59–81) residues 2–22, corresponding to T4 lysozyme residues 60–80. The amphipathic nature of the peptide is evident with the hydrophilic residues lying principally to the upper left of the wheel. The diagram was drawn with the program WHEEL, kindly provided by J. Segrest (Segrest *et al.*, 1990).

peptide. Asp12, which lies on the hydrophobic face of the helix, presents a potential disruption site as aspartate residues are known helix-breakers, especially along a hydrophobic face (Ptitsyn & Finkelstein, 1983; Huyghues-Despointes *et al.*, 1993). In contrast, the nearby Asp14 does not appear to disrupt the helix in solution. Asp14 possibly is less disruptive than Asp12 since it lies on the hydrophilic face of the helix, and in most solution structures, the side-chain carboxylate of Asp14 is in close enough proximity to form an $i,i+4$ helix-stabilizing salt bridge with the positively charged side chain of Arg18. A salt bridge in this position is also found in the X-ray structure (Weaver & Matthews, 1987). Asp3, also on the hydrophilic face, is at or next to the N-cap postion and may contribute to the helix stability by charge interactions with the helix dipole (Huyghues-Despointes *et al.*, 1993). From the unfavorable positioning of Asp12 in the helix, perhaps it is not surprising that some disruption occurs at this point, and in fact, the disruption is predicted by the ALB algorithm (Table 1; Ptitsyn & Finkelstein, 1983). However, this does not explain why the helix is less bent in the crystal.

Examination of the X-ray structure for T4 lysozyme reveals that the hydrophilic face of helix C is exposed, with the hydrophobic face oriented toward the protein interior (Weaver & Matthews, 1987). This places the negatively charged side chain of Asp70, corresponding to Asp12 in LYS(59–81), in a position to form a strong salt bridge with the positively charged side chain of His31 (Anderson *et al.*, 1990). This salt bridge, which contributes 3–5 kcal/mol toward the stabilization of the native structure, is placed against a rigid network of residues, which begins to form the hydrophobic core of the molecule (Anderson *et al.*, 1990). This combination of electrostatic and hydrophobic interactions presumably is responsible for the comparatively linear form of helix C seen in the X-ray structure of T4 lysozyme.

In summary, the study of LYS(59–81) provides an example of an isolated peptide fragment that, in an appropriate solution environment, can mimic the secondary characteristics of the corresponding region in the intact protein. The presence of significant populations of folded structures in a non-helix-stabilizing environment indicates that the peptide has a strong intrinsic propensity toward helix formation and supports the recent study that indicates that helix C forms relatively early in the folding of T4 lysozyme (Lu & Dahlquist, 1992).

ACKNOWLEDGMENT

We are grateful for the assistance of Dr. Andy Baxevanis, National Center for Biotechnology Information, in analyzing the CD data.

SUPPLEMENTARY MATERIAL AVAILABLE

NOESY spectra showing the medium range $H\alpha$–$H\beta_{i+3}$ and $H\alpha$–$H\gamma_{i+3}$ connectivities of LYS(59–81) in aqueous buffer and the NH–$H\alpha$ region of LYS(59–81) in SDS micelles (2 pages). Ordering information is given on any current masthead page.

REFERENCES

Anderson, D. E., Becktel, W. J., & Dahlquist, F. W. (1990) *Biochemistry 29*, 2403–2408.

Barlow, D. J., & Thornton, J. M. (1988) *J. Mol. Biol. 201*, 601–619.

Bradley, E. K., Thomason, J. F., Cohen, F. E., Kosen, P. A., & Kuntz I. D. (1990) *J. Mol. Biol. 215*, 607–622.

Braünschweiler, L., & Ernst, R. R. (1983) *J. Magn. Reson. 53,* 521–528.
Brooks, B. R., Bruccoleri, R. E., Olafson, B. D., States, D. J., Swaminathan, S., & Karplus, M. (1983) *J. Comput. Chem. 4,* 187–217.
Brown, J. E., & Klee, W. A. (1971) *Biochemistry 10,* 470–476.
Bruch, M. D., McKnight, C. J., & Gierasch, L. M. (1991) *Proteins: Struct., Funct., Genet. 10,* 130–139.
Brünger, A. T. (1992) *XPLOR Manual,* Yale University, New Haven, CT.
Brünger, A. T., Clore, G. M., Gronenborn, A. M., & Karplus, M. (1986) *Proc. Natl. Acad. Sci. U.S.A. 74,* 4130–4134.
Bycroft, M., Matouschek, A., Kellis, J. T., Jr., Serrano, S., & Fersht, A. R. (1990) *Nature 346,* 488–490.
Cavanagh, J., & Rance, M. (1992) *J. Magn. Reson. 96,* 670–678.
Chen, Y.-H., Yang, J. T., & Chau, K. H. (1974) *Biochemistry 13,* 3350–3359.
Chen, B.-L., Baase, W. A., Nicholson, H., & Schellman, J. A. (1992) *Biochemistry 31,* 1464–1476.
Clore, G. M., Brünger, A. T., Karplus, M., & Gronenborn, A. M. (1986) *J. Mol. Biol. 191,* 523–551.
Davis, D. G., & Bax, A. (1985) *J. Magn. Reson. 64,* 533–535.
Dyson, H. J., & Wright, P. E. (1991) *Annu. Rev. Biophys. Biophys. Chem. 20,* 519–538.
Dyson, H. J., Merutka, G., Waltho, J. P., Lerner, R. A., & Wright, P. E. (1992) *J. Mol. Biol. 226,* 795–817.
Endo, J., Shimada, I., Roise, D., & Inagaki, F. (1989) *Biochem. J. 106,* 396–400.
Goodman, E. M., & Kim, P. S. (1989) *Biochemistry 28,* 4343–4347.
Huyghues-Despointes, B. M. P., Scholtz, J. M., & Baldwin, R. L. (1993) *Protein Sci. 2,* 1604–1611.
Hyberts, S. G., Goldberg, M. S., Havel, T. F., & Wagner, G. (1992) *Protein Sci. 1,* 736–751.
Jasanoff, A., & Fersht, A. R. (1994) *Biochemistry 33,* 2129–2135.
Jiménez, M. A., Blanco, F. J., Rico, M., Santoro, J., Herranz, J., & Nieto, J. L. (1992) *Eur. J. Biochem. 207,* 39–49.
Kabsch, W., & Sander, C. (1983) *Biopolymers 22,* 2577–2637.
Kim, P. S., & Baldwin, R. L. (1982) *Annu. Rev. Biochem. 51,* 459–489.
Kraulis, P. J. (1991) *J. Appl. Crystallogr. 24,* 946–950.
Kumar, A., Ernst, R. R., & Wüthrich, K. (1980) *Biochem. Biophys. Res. Commun. 95,* 1–6.
Kuntz, I. D., Kosen, P. A., & Craig, E. C. (1991) *J. Am. Chem. Soc. 113,* 1406–1408.
Kuroda, Y. (1993) *Biochemistry 32,* 1219–1224.
Kuwajima, K. (1989) *Proteins: Struct., Funct., Genet. 6,* 87–103.
Ladbury, J. E., Hu, C.-Q., & Sturtevant, J. M. (1992) *Biochemistry 31,* 10699–10702.
Lu, J., & Dahlquist, F. W. (1992) *Biochemistry 31,* 4749–4756.
Mammi, S., & Peggion, E. (1990) *Biochemistry 29,* 5265–5269.
Matthews, B. W. (1993) *Annu. Rev. Biochem. 62,* 139–160.
McIntosh, L. P., Wand, A. J., Lowry, D. F., Redfield, A. G., & Dahlquist, F. W. (1990) *Biochemistry 29,* 6341–6362.
McLeish, M. J., Nielsen, K. J., Wade, J. D., & Craik, D. J. (1993) *FEBS Lett. 315,* 323–328.
Miranker, A., Radford, S. E., Karplus, M., & Dobson, C. M. (1991) *Nature 349,* 633–636.
Motta, A., Pastore, A., Gowd, N. A., & Castiglione Morelli, M. A. (1991) *Biochemistry 30,* 10444–10450.
Nilges, M., Gronenborn, A. M., Brünger, A. T., & Clore, G. M. (1988) *Protein Eng. 2,* 27–38.
Oas, T. G., & Kim, P. S. (1988) *Nature 336,* 42–48.
Osterhout, J. J., Jr., Baldwin, R. L., York, E. J., Stewart, J. M., Dyson, H. J., & Wright, P. E. (1989) *Biochemistry 28,* 7059–7064.
Padmanabhan, S., Marqusee, S., Ridgeway, T., Laue, T. M., & Baldwin, R. L. (1990) *Nature 344,* 268–270.
Pallaghy, P. K., Duggan, B. M., Pennington, M. W., & Norton, R. S. (1993) *J. Mol. Biol. 234,* 405–420.
Perczel, A., Park, K., & Fasman, G. D. (1992) *Anal. Biochem. 203,* 83–93.
Plateau, P., & Gueron, M. (1982) *J. Am. Chem. Soc. 104,* 7310–7311.
Ptitsyn, O. B. (1987) *J. Protein Chem. 6,* 273–293.
Ptitsyn, O. B., & Finkelstein, A. V. (1983) *Biopolymers 22,* 15–25.
Ptitsyn, O. B., Pain, R. H., Semisotnov, G. V., Zerovnik, E., & Razgulyaev, O. I. (1990) *FEBS Lett. 12,* 20–24.
Rance, M., Sorenson, O. W., Bodenhausen, G., Wagner, G., Ernst, R. R., & Wüthrich, K. (1983) *Biochem. Biophys. Res. Commun. 117,* 479–485.
Rizo, J., Blanco, F. J., Kobe, B., Bruch, M. D., & Gierasch, L. M. (1993) *Biochemistry 32,* 4881–4894.
Roder, H., Elöve, G. A., & Englander, S. W. (1988) *Nature 335,* 700–704.
Sauer, U. H., Dao-pin, S., & Matthews, B. W. (1992) *J. Biol. Chem. 267,* 2393–2399.
Segawa, S. I., Fukuno, T., Fujiwara, K., & Noda, Y. (1991) *Biopolymers 31,* 497–509.
Segrest, J. P., De Loof, H., Dohlman, J. G., Brouilette, C. G., & Anantharamiah, G. M. (1990) *Proteins: Struct., Funct., Genet. 8,* 103–117.
Shoemaker, K. R., Kim, P. S., York, E. J., Stewart, J. M., & Baldwin, R. L. (1987) *Nature 326,* 563–567.
Sönnichsen, F. D., van Eyk, J. E., Hodges, R. S., & Sykes, B. D. (1992) *Biochemistry 31,* 8790–8798.
Staley, J. P., & Kim, P. S. (1990) *Nature 344,* 685–688.
Sundaralingham, M., & Sekharudu, Y. C. (1989) *Science 244,* 1333–1337.
Tirado-Rives, J., & Jorgensen, W. L. (1991) *Biochemistry 30,* 3864–3871.
Udgaonkar, J. B., & Baldwin, R. L. (1988) *Nature 335,* 694–699.
Wade, J. D., Fitzgerald, S. P., McDonald, M. R., McDougall, J. G., & Tregear, G. W. (1986) *Biopolymers 25,* S21–S37.
Waltho, J. P., Feher, V. A., Merutka G., Dyson, H. J., & Wright P. E. (1993) *Biochemistry 32,* 6337–6347.
Weaver, L. H., & Matthews, B. W. (1987) *J. Mol. Biol. 193,* 189–199.
Wishart, D. S., Sykes, B. D., & Richards, F. M. (1991) *J. Mol. Biol. 222,* 311–333.
Woody, R. W. (1985) *The Peptides* (Hruby, V., Ed.) Vol. 7, Academic Press, New York.
Wu C.-S. C., & Yang, J. T. (1978) *Biochem. Biophys. Res. Commun. 82,* 85–91.
Wu, C.-S. C., Hachimori, A., & Yang, J. T. (1982) *Biochemistry 21,* 4556–4562.
Wüthrich, K. (1986) *NMR of Proteins & Nucleic Acids,* John Wiley & Sons, New York.
Wüthrich, K., Billeter, M., & Brown, W. (1983) *J. Mol. Biol. 169,* 949–961.
Yang, J. T., Wu, C.-S. C., & Martinez, H. M. (1986) *Methods Enzymol. 130,* 208–269.
Zhou, N. E., Zhu, B.-Y., Sykes, B. D., & Hodges, R. S. (1992) *J. Am. Chem. Soc. 114,* 4320–4326.
Zhou, N. E., Kay, C. M., Sykes, B. D., & Hodges, R. S. (1993) *Biochemistry 32,* 6190–6197.